European Conference on Computational Fluid Dynamics
ECCOMAS CFD 2006
P. Wesseling, E. Oñate and J. Périaux (Eds)

PARTICLE SEDIMENTATION IN WALL-BOUNDED TURBULENT FLOWS

M. Cargnelutti*, W.A. Breugem†, L. M. Portela *, R.F. Mudde*, W.S.J. Uijttewaal†, G.S. Stelling†

*Delft University of Technology, Faculty TNW
Prins Bernhardlaan 6, 2628 BW, The Netherlands
e-mail: m.f.cargnelutti@tnw.tudelft.nl
web page: http://www.msp.tudelft.nl
†Delft University of Technology, Faculty CiTG,
Stevinweg 1, 2628 CN Delft, The Netherlands

Key words: Particle-laden flows, turbulence, DNS, PIV

Abstract. *In this work, a comparison between the results of point-particle direct numerical simulations and PIV/PTV experiments of a particle-laden horizontal channel flow is presented. The numerical simulations were preformed trying to mimic as much as possible the experimental conditions. The accuracy of the point-particle approach was evaluated by comparison of the concentration, velocity and velocity fluctuation profiles. The agreement was good, both qualitatively and quantitatively, in the central part of the channel. However, in the near-wall region some differences were found. This can be explained by the lack of resuspension present in the simulations, because we considered only the fluid-particle interaction (one-way coupling) and neglected both the particle-fluid interaction (two-way coupling) and the particle-particle interaction (collisions).*

1 INTRODUCTION

The transport of sediment in wall-bounded turbulent flows is important in numerous engineering applications. A common situation involves the transport and sedimentation of sand-like particles it turbulent water-flows. The sedimentation of the particles depends strongly on the interaction between the particles and the turbulence, and there is a lack of good understanding about it. Most of the work done so fas has been on solid particles in air, with a density ratio between the particle and the fluid $\rho_p/\rho_f \sim 1000$[1]. Here we are interested in a density ratio $\rho_p/\rho_f \sim 1$. One technique used to simulate the particle-fluid interaction in a turbulent flow is called fully-resolved turbulence[2]. In that case, all the turbulent scales of the flow around each particle are solved. This type of simulations is computationally very expensive, and currently impossible to use for a large number of particles. Another techniques used to simulate the motion of particles in a turbulent flow is the point-particle approach[3] . In this approach, all is needed

to calculate the forces on a particle is the fluid-velocity interpolated at the center of the particle. The advantage of this approach is that it is computationally fast, and allows us to simulate millions of particles with a small computational cost. A drawback is that the particles must be significantly smaller than the smallest turbulence scales. Even though point-particle simulations are well known, it is not clear to what extent the restriction in the particle size can affect the accuracy of the simulations. A major problem in the validation of point-particle simulations is a lack of reliable experimental data. A difficulty is that the experimental conditions must be compatible with the point-particle approach requirements (i.e., the particles can not be "large"). In this work, in order to evaluate the accuracy of the point-particle approach, we performed point-particle DNS simulations of a particle-laden turbulent open-channel flow, and compared the results with PIV/PTV experiments. The simulations were performed trying to mimic as much as possible the experimental conditions, which were compatible with the point-particle approach requirements. The comparison between the experiments and the simulations was used to evaluate the possibilities and limitations of the point-particle approach.

The layout of the paper is as follows. In section 2 there is a description of the forces acting on the particles, and the particle equation of motion. In sections 3 and 4 the experimental and numerical details are explained. A comparison of the results of the simulations and experiments is presented in section 5, and finally the conclusions are presented in section 6.

2 Particle Laden Flow

In a particle-laden flow we have two phases present in the domain of interest: a continuous phase (fluid) and a dispersed phase (particles). Assuming the flow is incompressible, the continuous phase can be represented with the Navier-Stokes equations:

$$\nabla \cdot \vec{u} = 0 \tag{1}$$

$$\frac{D\vec{u}}{Dt} = -\frac{\nabla P}{\rho_f} + \nu \nabla^2 \vec{u} \tag{2}$$

where $\vec{u}$ is the fluid velocity, P the pressure, ρ_f the fluid density, and ν the fluid kinematic viscosity.

The forces acting on a particle immersed in a flow were described properly by Maxey and Riley in 1983[4]. For the present case of small light particles in water, with particle Reynolds number smaller than one, the lift and Basset forces can be neglected. Considering Stokes drag, gravity, added mass and the surrounding fluid stress, the motion of a particle is described by:

$$\rho_p \frac{\pi d_p^3}{6} \frac{d\vec{u}}{dt} = \underbrace{3\pi\mu d_p \left(\vec{u} - \vec{v}\right)}_{Drag} + \underbrace{\rho_p \frac{\pi d_p^3}{6} \vec{g}}_{Gravity} + \underbrace{\frac{\pi d_p^3}{6} \left(\nabla \cdot \vec{\vec{T}}\right)}_{Stresses} + \underbrace{\frac{\rho_f}{2} \frac{\pi d_p^3}{6} \left(\frac{D\vec{u}}{Dt} - \frac{d\vec{v}}{dt}\right)}_{Added\,mass} \tag{3}$$

In this case, ρ_p is the particle density, d_p is the particle diameter, μ is the fluid viscosity, $\vec{g}$ is the gravity acceleration, and $\vec{u}$ and $D\vec{u}/Dt$ are the surrounding fluid velocity and acceleration respectively at the particle position, and $\vec{\vec{T}}$ is the fluid stress tensor. Neglecting the influence of the particles on the fluid, the acceleration of the surrounding fluid is given by

$$\frac{D\vec{u}}{Dt} = \frac{\partial \vec{u}}{\partial t} + \vec{u} \cdot (\nabla \vec{u}) = \frac{1}{\rho_f} \left(\nabla \cdot \vec{\vec{T}} \right) + \vec{g} \tag{4}$$

Finally, we can express the particle equation of motion as

$$\frac{d\vec{v}}{dt} = \frac{1}{\tau_a} (\vec{u} - \vec{v}) + \frac{\beta - 1}{\beta + \frac{1}{2}} \vec{g} + \frac{3}{2} \frac{1}{\beta + \frac{1}{2}} \frac{D\vec{u}}{Dt} \tag{5}$$

were $\beta = \rho_p / \rho_f$ is the particle-fluid density ration, and the particle relaxation time τ_p and τ_a are given by

$$\tau_p = \beta \frac{d_p^2}{18\nu} \tag{6}$$

$$\tau_a = \frac{\beta + \frac{1}{2}}{\beta} \tau_p \tag{7}$$

3 Experimental Setup

The experiments were performed in an open channel, with a length of 23.5 m a width of 0.495 m and a height of 0.50 m (Fig. 1). The walls and bottom were made of glass in order to have a hydraulically smooth boundary. The water was pumped from a buffer into the flume. At the downstream side, the water level was controlled with an adjustable weir, followed by three pipes allowing the water to return to the buffer. In order to perform the fluid velocity measurements, the water was seeded with 10 μm hollow glass spheres ($\rho = 1100\ kg/m^3$).

As pseudo-sediment, 347 μm ($\sigma = 45\ \mu m$) polystyrene particles were used, which had a density ρ_p of 1035 kg/m^3. We measured a terminal velocity v_T of 2.2 mm/s, which compares well with the theoretical estimate of 2.1 mm/s ($Re_p = v_T d_p / \nu_f = 0.71$). The particles were fed to the channel with a particle feeder. The sediment mixture entered the channel through a nozzle with an inner diameter of 1 cm at the channel's centerline and its center located at 0.7 cm below the free surface. The inflow velocity was adjusted to the channel velocity.

The measurement section was located at a distance of 14.25 m from the channel entrance. At this location, a combination of both PIV and PTV was used to measure the velocities of the polystyrene particles and the fluid.

Three sets of experimental data were collected. All of these sets were measured at $Re = 10,000$ ($Re_* = 508$), which was obtained by setting the centerline velocity to

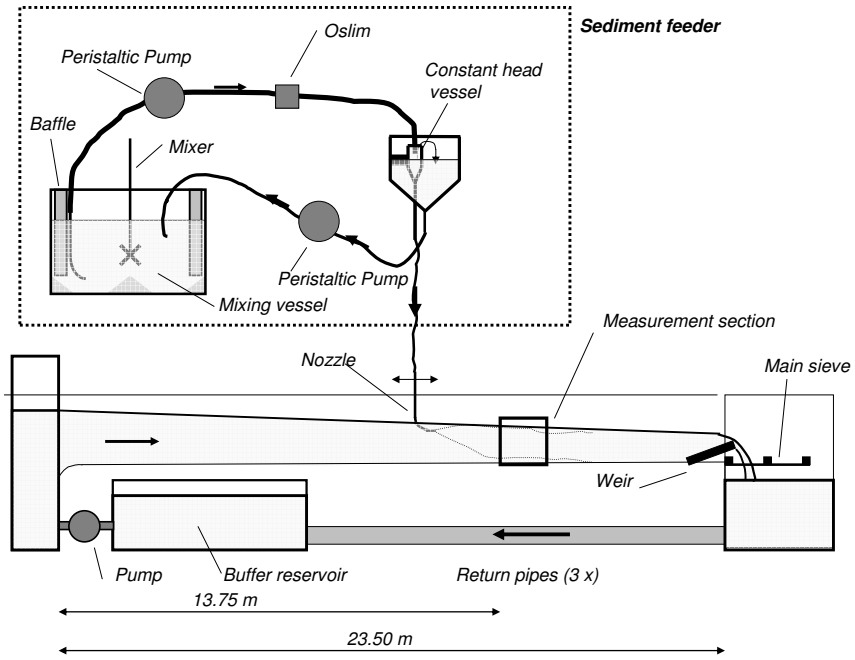

Figure 1: Experimental setup.

0.20 m/s and the water depth to 0.050 m. This velocity was chosen to ensure a sufficient amount of sediment in the water column ($u_*/v_T \approx 5$). The only variable that was changed between these sets was the position of the nozzle, which was placed at 80 cm, 175 cm and 375 cm from the measurement section, i.e. at $x_{in}/h = 16$, $x_{in}/h = 35$ and $x_{in}/h = 75$. During the measurements, it appeared that the discharge from the nozzle in the $x_{in}/h = 16$ case was somewhat lower than in the other cases. The volumetric sediment concentration in the mixing vessel was $1.2\ 10^{-2}$.

The data were processed with a modified version of the method of Kiger[5] to discriminate between sediment and tracer particles. Then, a PTV algorithm was used to calculate the positions and velocity of the sediment particles, whereas the fluid velocity was calculated from the tracer image with PIV.

A more complete description of the experimental set-up is presented in reference[6].

4 Numerical Method

We performed DNS simulations of a particle-laden open channel flow, as can be seen in figure 2. We imposed a free-slip boundary condition at the top wall, which mimicked the experimental situation, since the free surface was approximately flat. A no-slip condition was imposed at the bottom-wall. In the stream and span wise directions we used periodic boundary conditions. The flow was driven by a stream wise pressure gradient. The code used was a standard finite-volume code on a staggered grid. The continuous phase is solved using a predictor-corrector solver, with a second-order Adams-Bashforth scheme.

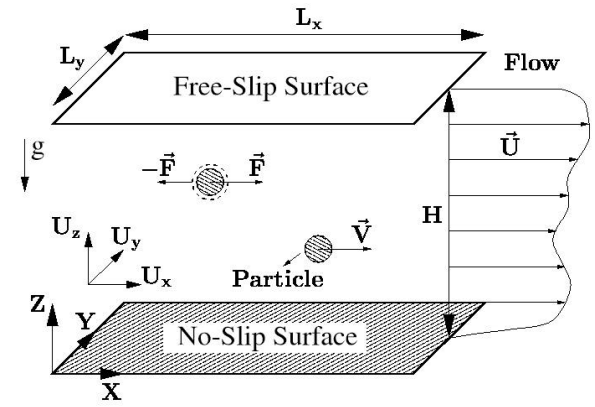

Figure 2: Open-channel domain

The time step is obtained using the Courant stability criterion[3].

The equations of motion were made dimensionless using the friction velocity u_τ and the height of the channel H. With this parameters, the Reynolds number was set to $Re_\tau = 500$. This gave us a bulk Reynolds number of around $Re_b = 10.000$. In the present simulations, we considered water as the fluid phase, with a viscosity of 1.01 $10^{-6} m^2/s$. The particle-fluid density ratio β was set to 1.0367.

The simulations were performed in dimensionless units. The computational domain was 5 x 2 x 1 in channel height units, in the stream (x), span (y) and normal wise direction (z) respectively. This gave a domain of 2.500 x 1.00 x 500 in wall units. We used a grid of 256 x 192 x 128 nodes. The grid was uniform in the x and y directions, with $\Delta x^+ \sim 10$ and $\Delta y^+ \sim 5$ in wall units. A hyperbolic-tangent stretching was used for the normal direction. This leaded to a grid spacing of $\Delta z^+ \sim 0.9$ at the wall, and $\Delta z^+ \sim 7$ at the center of the channel. The stretching factor used was 1.7. With this resolution we were able to solve all the smallest scales of the flow[7]. For the discrete phase, we integrated the particle equation of motion using a explicit method. To calculate the fluid velocity at the particle position we used a tri-linear interpolation method.

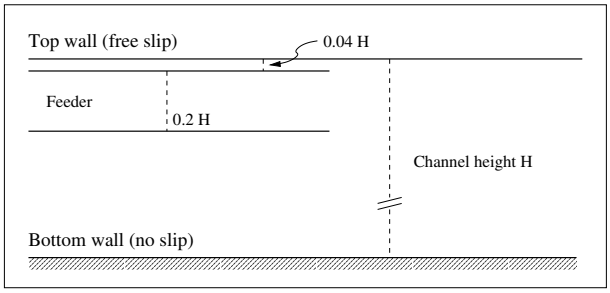

Figure 3: Side view of the channel

In order to mimic the experiments, we released the particles in an horizontal slab (see

figure 3) of the same height as the particle injector in the experiments. We released the particles in an homogeneous distribution inside the slab with the initial velocity equal to the surrounding fluid. Each particle was tracked across the channel. Because of the periodicity of the domain, when a particle left the channel from one side, it was re-injected at the opposite side of the channel. We kept on tracking the distance traveled by each particle, and computed the concentration profiles and velocity distributions at the same position as in the experiments. By this we mean that, for each particle, we collected the particle position and velocity when they crossed the measurement point in the experimental part, i.e., when the particle had traveled a distance equal to 16, 35 and 75 water depths. All the quantities were averaged according to the particle density presented in the measurement point.

5 Results

The results of both the experiments and the simulations are presented in this section. All the results are presented at the tree different measurement points: at 16, 35 and 75 water depths. The results plotted on the left hand side of the figures correspond to experimental values, while those on the right hand side show the corresponding numerical calculations.

5.1 Concentration profiles

In figure 4 are presented the concentration profiles, normalized with the concentration value at a fix distance from the wall, in this case, at $z^+ = 36$.

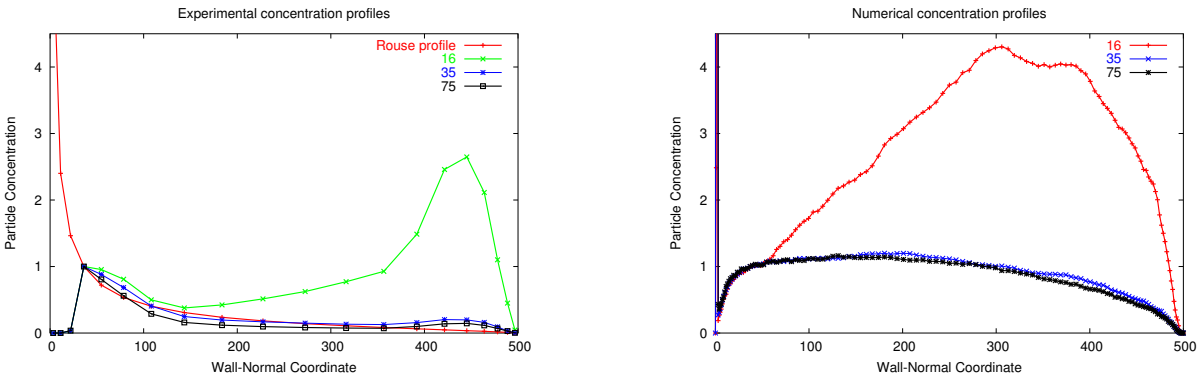

Figure 4: Concentration profiles

In this case, there is not an exact match in the results. At 16 water depths in both cases (experimental and numerical) there is a peak of concentration around the injection region, because the concentration profiles were still developing.

The experimental concentrations show a Rouse-like profile at a distance higher that 35 water depths, with an exponential decline. In the numerical calculations, on the other

hand, at the same distances from the injection point the concentration is approximately uniform at the center of the channel, it decreases toward the wall, and it is huge at the bottom wall. Note that the simulations were done using a point-particle approach, with one-way coupling only. This means that the particles do not interact with each other, and they can occupy the same physical space (actually they do when they are at the wall). The use of this conditions in the simulations explains the discrepancy in the concentration profiles. The particle resuspension process relied only on the vertical fluid velocity fluctuations, which were not strong enough to lift the particles up into the central part of the channel. When the particles are at rest at the bottom wall, the fluid velocity at the center of the particle needed to over come the gravity effect was $w'_f > 0.24$, while the average fluid velocity fluctuation at the same point was $w'_f \sim 0.03$. For this reason, there was hardly any resuspension in the numerical simulations. In case of the experiments, the particle concentration at the bottom of the channel is not only high enough to encourage resuspension due to the large gradient of concentration, but also the inter particle-collision rate increases and plays an important roll in the resuspension process.

As the concentration at the bottom increases, the boundary condition at the bottom of the channel is more likely to be represented properly in the numerical simulations by using absorbing walls instead of bouncing walls. In case of using bouncing walls, there are two alternatives to try to mimic closely the real situation: either the inter particles collisions should be considered, or an ad hoc resuspension model has to be implemented. We are currently working on the implementation of this different numerical conditions.

5.2 Velocity profiles

In figure 5 and 6, the mean stream and normal wise velocity profiles are shown respectively. As with the concentration profiles, the plots on the left hand side of the figure correspond to the experimental data, and the plots on the right hand side correspond to numerical simulations. In case of the velocity profile, for both experiments and simulations there are three plots for each quantity. The first one corresponds to the profiles computed with particles that had traveled a distance equal to 16 water depths, the second plot to a distance of 35 water depths, and the third and last one corresponds to a distance equal to 75 water depths.

In the mean stream wise velocity profiles it can be seen that there is a good agreement between the experimental and numerical profiles. In both cases, at the first measurement point the particle velocity is higher that the fluid, because the particles are coming from the top part of the channel, a region of higher mean velocity. Even though the particle relaxation time is quite low, the particles are moving downward mainly in regions of high vertical fluid velocity. For this reason, the stream wise average particle velocity is higher than the stream wise fluid velocity at the first measurement point.

As we move on to the next measurement points, the stream wise particle velocity slows down, and at the last measurement point, its value it is almost equal (for the simulations) or lower (for the experiments) than the fluid velocity. The reason for this difference is that

for the experiments, at the last measurement point the particle diffusion from the bottom wall to the center is important. The particles tend to be preferentially concentrated in the ejections more than in sweeps, which leads to a slower mean velocity. For the simulations, instead, because there is almost no diffusion from the bottom wall, the particle tend to be more uniform distributed at the last measurement point, and the particle mean velocity almost equals the fluid velocity.

In the case of the mean normal velocity profiles (see figure 6), the agreement is not perfect. At the first measurement point, in both experiment and simulations the particle vertical velocity is higher that the fluid (which can be considered zero within the error bars). The magnitude of the particle velocity is similar for both cases. At the second and third measurement point, the experimental particle vertical velocity is close to zero, while the numerical value is still around the terminal velocity in stagnant medium. This is also due to the lack of diffusion from the bottom wall in the simulations, which will create a steady state particle distribution across the vertical direction in the channel, with a zero mean vertical velocity.

The experimental and numerical velocity fluctuation profiles show a good agreement, qualitatively and quantitatively, as can be seen in figures 7 and 8. In the stream wise direction, the particle velocity fluctuations are similar to the fluid velocity fluctuation in the central part of the channel. In the near wall region, the numerical values of the particle velocity fluctuations are smaller than the fluid, because of the lack of inter particle collisions.

The vertical particle velocity fluctuations are quite similar to the fluid velocity fluctuations for both experiments and simulations. In the experimental case, the particle fluctuations are slightly higher than the fluid fluctuations, which is an indication that, since the particle concentration is higher in that region, two-way coupling effects are modifying the results. This is not present in the simulations, that were performed using one-way coupling.

For both experiments and simulations, the particle Reynold stresses $< u'v' >$ are higher than the fluid values in the central part of the channel at the first measurement point. Later on, in the next measurement regions, the particle Reynolds stresses slow down their value till almost the same as the fluid Reynolds stresses. The difference in the first measurement region is due that in the beginning, the particles are preferentially concentrated in regions of downward vertical fluid velocity. This increases the Reynolds stresses, because the particles are not found in ejection, which are the coherent structures which add most to the Reynolds stresses, because they are intenser than sweeps[8].

6 CONCLUSIONS

We presented in this paper a comparison between experiments and simulations of a particle-laden turbulent-horizontal channel flow. The results of the comparison of the experiments and simulations showed a good agreement, both qualitatively and quantitatively. In the near-wall region we found a mismatch in the comparison. In order to

obtain a closer-match, a resuspension mechanism has to be implemented in the numerical simulations, either by the use of an ad-hoc resuspension model, or by the inclusion of collisions. However, besides the differences we found, with the use of a point-particle approach we were able to represent the experimental situation. This approach showed to be accurate and computationally cheap, in comparison with fully-resolved simulations.

7 ACKNOWLEDGMENTS

We acknowledge the financial support provided by STW, WL—Delft Hydraulics and KIWA Water Research. The numerical simulations were performed at Sara, and the computational time was provided by NWO.

REFERENCES

[1] S.L. Anderson and E.K. Longmire. Interpretation of piv autocorrelation measurements in complex particle-laden flows. *Experiments in Fluids*, 20:314–317, 1996.

[2] T.M. Burton and J.K. Eaton. Fully resolved simulation of particle-turbulence interaction. *Journal of Fluid Mechanics*, 545:67–111, 2005.

[3] L.M. Portela and R.V.A. Oliemans. Eulerian-lagrangian dns/les of particle-turbulence interactions in wall-bounded flows. *International Journal for Numerical Methods in Fluids*, 9:1045 – 1065, 2003.

[4] M.R. Maxey and J.J. Riley. Equation of motion for a small rigid sphere in a nonuniform motion. *Physics of Fluids*, 26(4):883–889, 1983.

[5] K.T. Kiger and C. Pan. Piv technique for the simultaneous measurement of dilute two-phase flows. *Journal of Fluids Engineering*, 122:811–818, 2000.

[6] W.A. Breugem and W.S.J. Uijttewaal. A piv/ptv experiment on sediment transport in an horizontal open channel flow. *Proceedings of the International Conference on Fluvial Hydraulics River Flow 2006*, 2006.

[7] H. Abe, H. Kawamura, and Y. Matsuo. Direct numerical simulation of a fully developed turbulent channel flow with respect to the reynolds number dependence. *Journal of Fluids Engineering*, 123:382–393, 2001.

[8] I. Nezu and H. Nakagawa. *Turbulence in Open-Channel Flows*. A.A. Balkema, 1993.

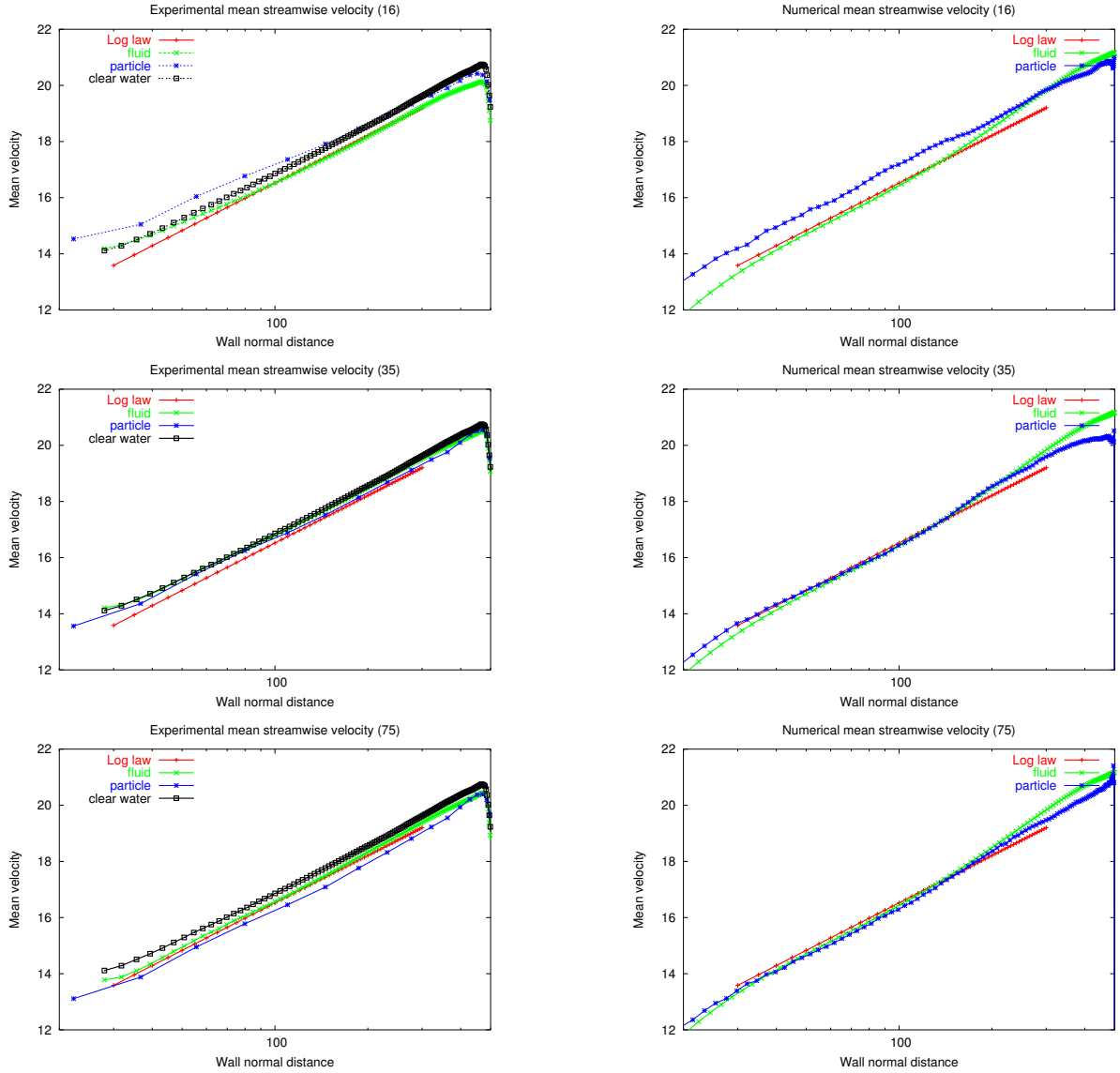

Figure 5: Mean stream wise velocity profiles

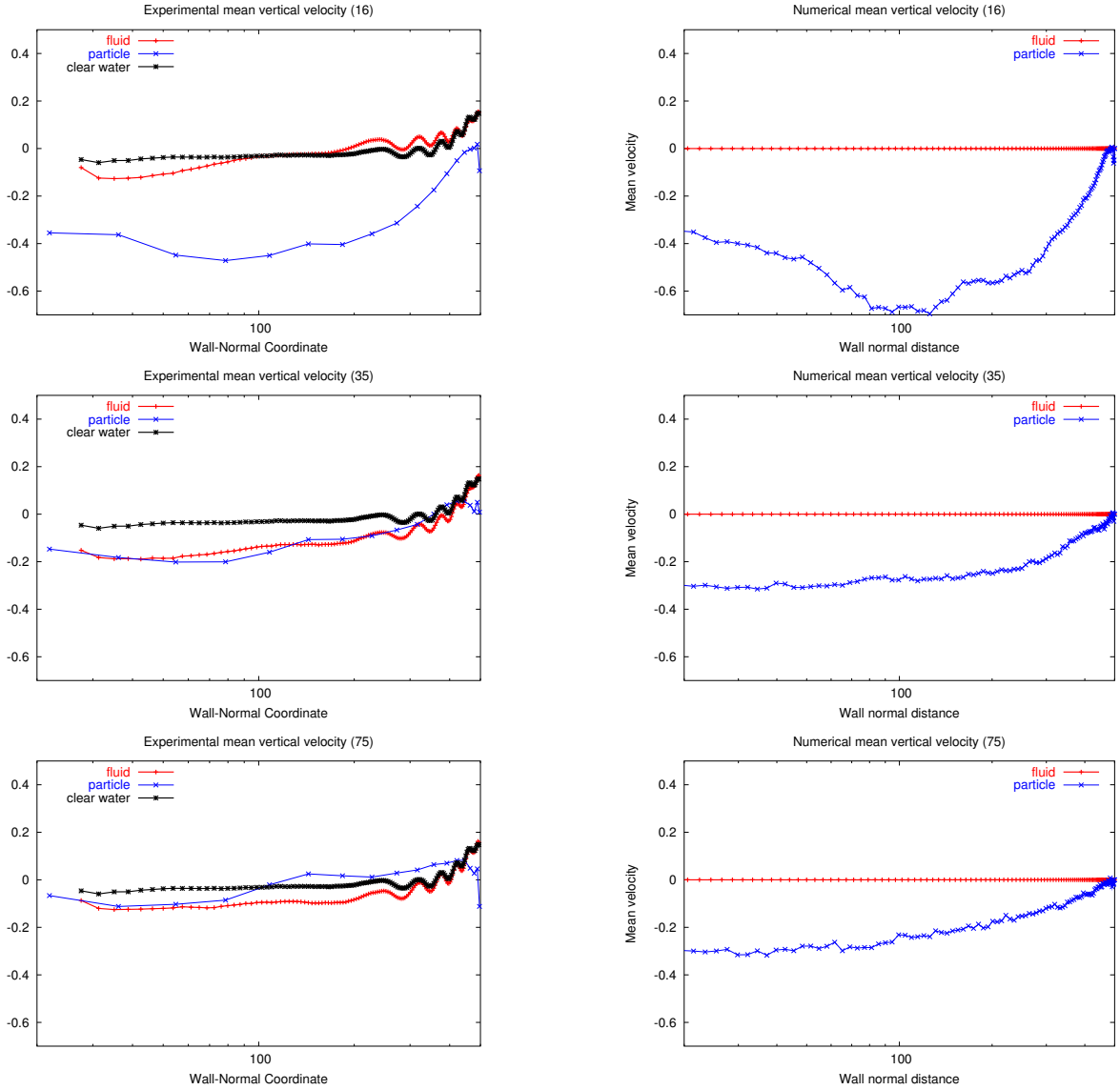

Figure 6: Mean normal wise velocity profiles

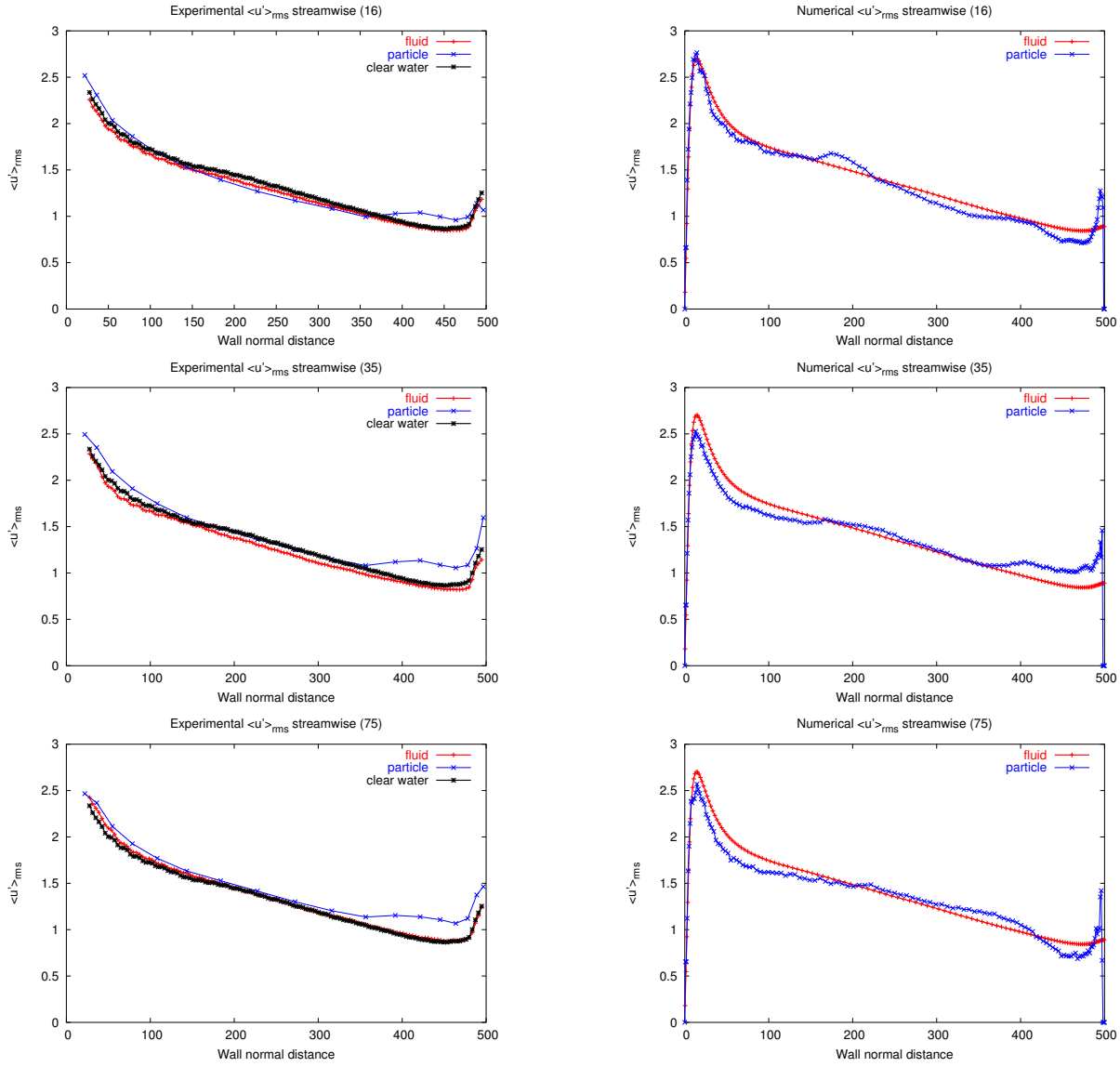

Figure 7: Stream wise velocity fluctuations

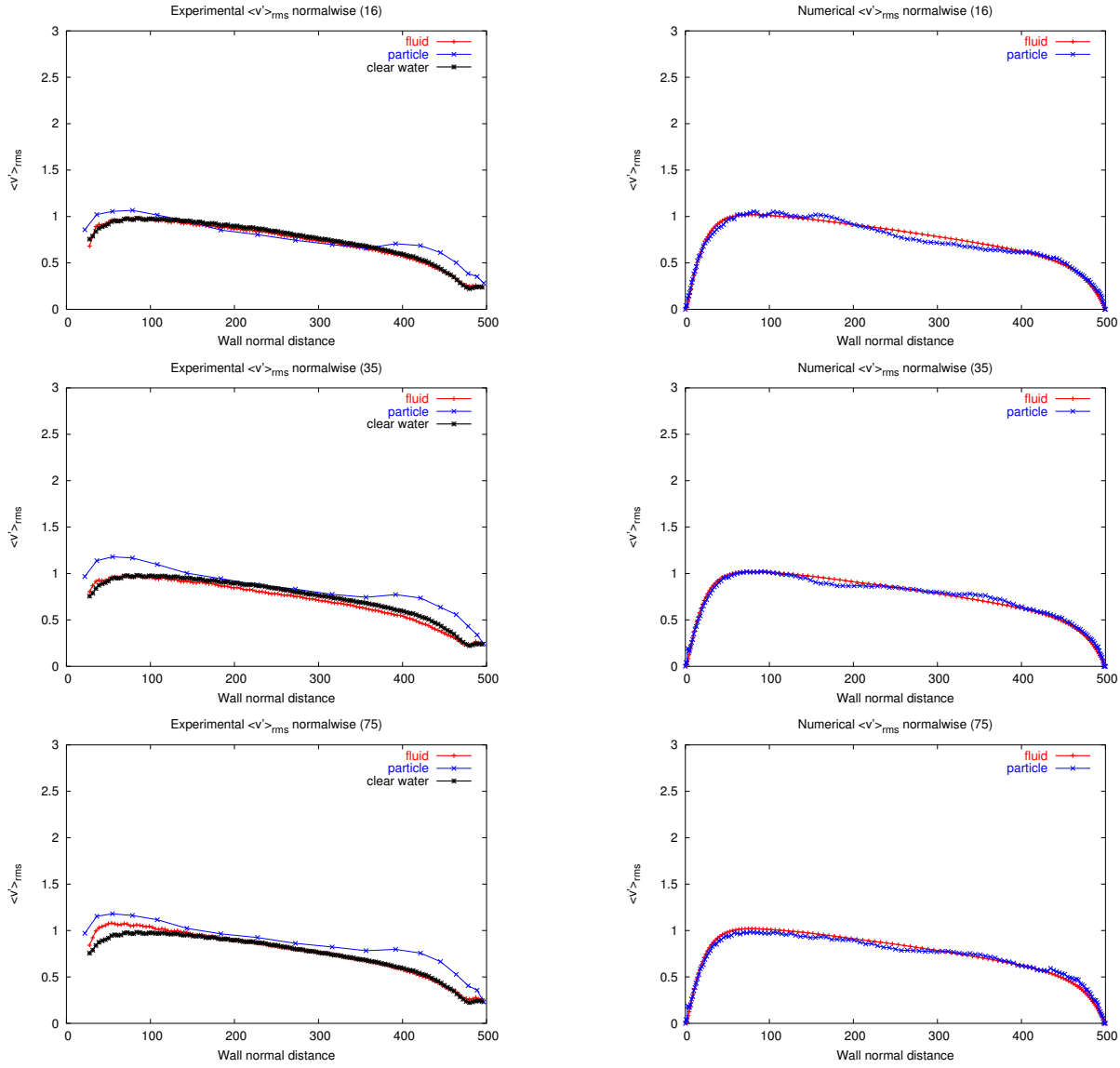

Figure 8: Normal wise velocity fluctuations

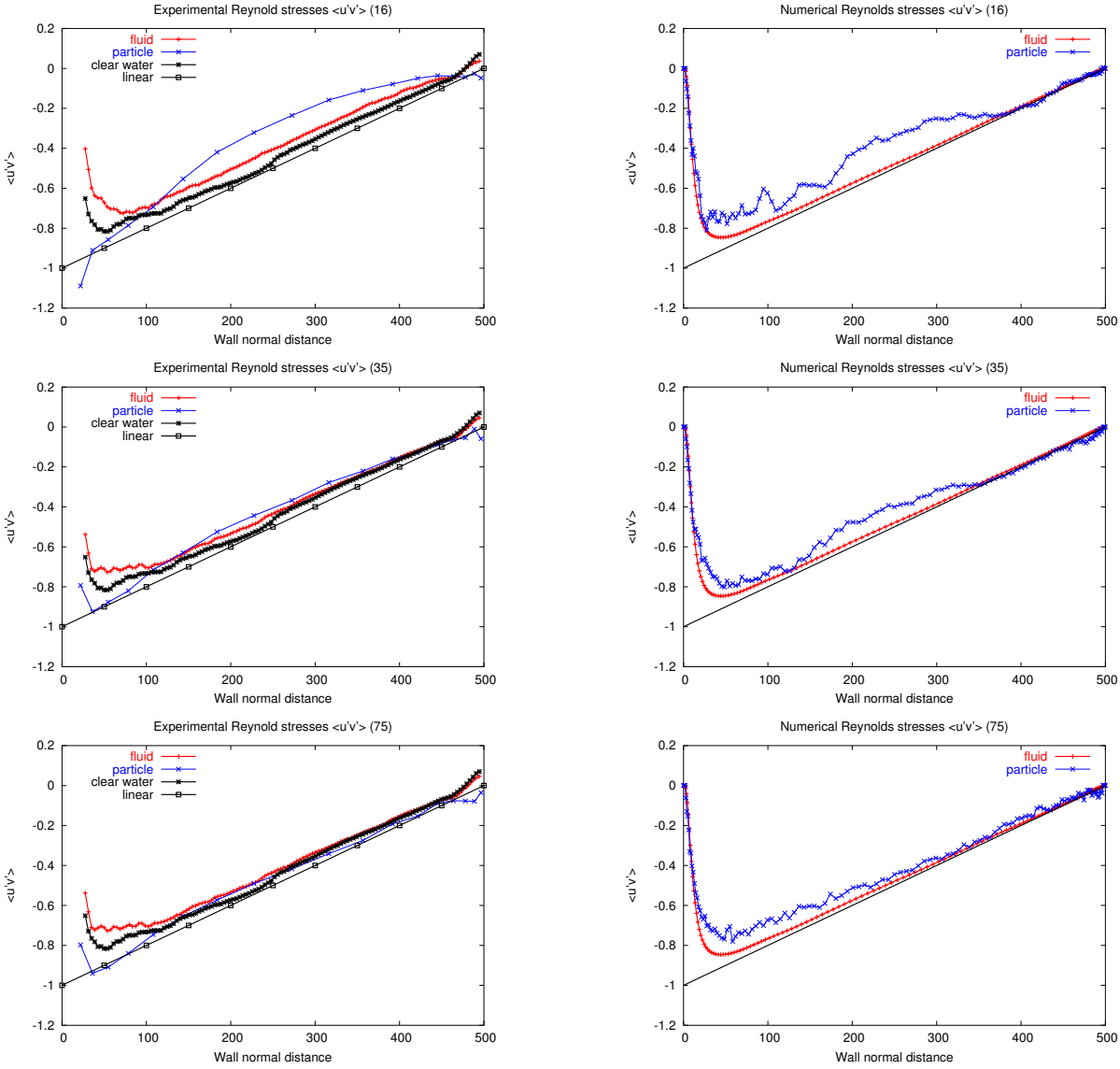

Figure 9: Reynolds stresses $< u'v' >$